Physics Letters B 754 (2016) 26–32

Contents lists available at ScienceDirect

Physics Letters B

www.elsevier.com/locate/physletb

Formation spectra of charmed meson–nucleus systems using an antiproton beam

J. Yamagata-Sekihara [a], C. Garcia-Recio [b], J. Nieves [c], L.L. Salcedo [b], L. Tolos [d,e]

[a] National Institute of Technology, Oshima College, Oshima, Yamaguchi, 742-2193, Japan
[b] Departamento de Física Atómica, Molecular y Nuclear, and Instituto Carlos I de Física Teórica y Computacional, Universidad de Granada, E-18071 Granada, Spain
[c] Instituto de Física Corpuscular (centro mixto CSIC-UV), Institutos de Investigación de Paterna, Aptdo. 22085, 46071, Valencia, Spain
[d] Institute de Ciencias del Espacio (IEEC/CSIC), Campus UAB, Carrer de Can Magrans s/n, 08193 Cerdanyola del Valles, Spain
[e] Frankfurt Institute for Advanced Studies, Johann Wolfgang Goethe University, Ruth-Moufang-Str. 1, 60438 Frankfurt am Main, Germany

ARTICLE INFO

Article history:
Received 11 December 2015
Received in revised form 6 January 2016
Accepted 6 January 2016
Available online 8 January 2016
Editor: W. Haxton

Keywords:
Charmed mesic nuclei
Formation spectra
DN and $\bar{D}N$ interaction
Klein–Gordon equation
Green's function method

ABSTRACT

We investigate the structure and formation of charmed meson–nucleus systems, with the aim of understanding the charmed meson–nucleon interactions and the properties of the charmed mesons in the nuclear medium. The $\bar{D}$ mesic nuclei are of special interest, since they have tiny decay widths due to the absence of strong decays for the $\bar{D}N$ pair. Employing an effective model for the $\bar{D}N$ and DN interactions and solving the Klein–Gordon equation for $\bar{D}$ and D in finite nuclei, we find that the D^-–^{11}B system has 1s and 2p mesic nuclear states and that the D^0–^{11}B system binds in a 1s state. In view of the forthcoming experiments by the PANDA and CBM Collaborations at the future FAIR facility and the J-PARC upgrade, we calculate the formation spectra of the [D^-–^{11}B] and [D^0–^{11}B] mesic nuclei for an antiproton beam on a ^{12}C target. Our results suggest that it is possible to observe the 2p D^- mesic nuclear state with an appropriate experimental setup.

1. Introduction

The study of hadronic atoms provides essential information on the properties of hadron–nucleon interactions, hadrons in matter as well as the properties of nuclei that are not accessible by other probes. Pionic and kaonic atoms have been intensively investigated over the years [1–6], whereas antiprotons in atoms have become a matter of recent interest [7–9].

In view of the forthcoming experiments by the PANDA and CBM Collaborations at the future FAIR facility [10] and the J-PARC upgrade [11], the attention has been also focused on charmed meson–nucleus systems. One of the first works on charmed mesic nuclei analyzed the possibility of D^- atoms [12]. There, the 1s, 2s and 1p states of D^- in ^{208}Pb were evaluated using the quark–meson coupling model of Ref. [13]. The energy levels of the $\bar{D}$ meson in ^{208}Pb and ^{40}Ca were obtained in [14] within a model for the charmed meson–nucleon interaction based on the pion exchange. Also, $\bar{D}NN$ and $\bar{D}^*NN$ bound states were predicted in [15,16] as well as a bound state of DNN in [17].

All these works rely upon building a realistic charmed meson–nucleon interaction and extending the analysis to the nucleus. In that respect, unitarized meson–baryon coupled-channel approaches including the charm degree of freedom have been very successful [18–35]. However, these models do not explicitly incorporate heavy-quark spin symmetry (HQSS) [36–38] and, thus, it is unclear whether they fulfilled the constraints imposed by HQSS. HQSS is a QCD symmetry that appears when the quark masses, such as the charm mass, become larger than the typical confinement scale.

The implementation of HQSS constraints on the meson–baryon interactions with heavy-quark degrees of freedom has been more recently studied in [39–46]. Among these works, we must highlight those based on an extension of the Weinberg–Tomozawa (WT) interaction to spin-flavor including HQSS constraints [39–44]. Within this approach, we have analyzed the properties of D and $\bar{D}$ as well as D^* and $\bar{D}^*$ in dense matter and studied the formation of charmed-meson nucleus bound states [47–49].

In Ref. [48] we have obtained that D^0 binds weakly with nuclei, in contrast to [12], while the D^0-nucleus states have significant widths, in particular for heavy nuclei such as ^{208}Pb. The best chances for observation of bound states are in the region of ^{24}Mg,

E-mail address: yamagata@oshima-k.ac.jp (J. Yamagata-Sekihara).

http://dx.doi.org/10.1016/j.physletb.2016.01.003

provided an orbital angular momentum separation can be done. Moreover, only D^0-nucleus bound states are possible since the Coulomb interaction prevents the formation of observable bound states for D^+ mesons. With regard to $\bar{D}$-mesic nuclei, not only D^- but also $\bar{D}^0$ bind in nuclei [49]. The spectrum contains states of atomic and of nuclear types for all nuclei for D^- whereas only nuclear states are present for $\bar{D}^0$ in nuclei, as expected. Compared to the pure Coulomb levels, the atomic states are less bound. The nuclear ones are more bound and may present a sizable width. Moreover, nuclear states only exist for low angular momenta.

In this work, we continue these previous studies and investigate the possibility of observing D^-–^{11}B and D^0–^{11}B bound states in ^{12}C$(\bar{p}, D^+)$ and ^{12}C$(\bar{p}, \bar{D}^0)$ nuclear reactions. The formation spectra are calculated with the Green's function method. This is the first attempt to calculate the formation spectra for charmed mesic nuclear states with an energy dependent optical potential coming from the charmed meson–nucleon interaction in matter. Throughout this study, we set the incident antiproton beam at 8 GeV/c and the final-state D^+ and $\bar{D}^0$ mesons to go forward direction, in an attempt to give useful information to experiments with antiprotons beams, such as PANDA (FAIR) and J-PARC.

This paper is organized as follows. In Sec. 2 we present the formation spectra in terms of the production cross sections of the $(\bar{p}, D^+)$ and $(\bar{p}, \bar{D}^0)$ reactions on a nuclear target. We also describe the DN and $\bar{D}N$ effective interactions in medium together with the D and $\bar{D}$ self-energies and optical potentials used in this study. Details on the construction of the nuclear density to evaluate the optical potentials for a given nucleus are presented in Appendix A. Next, in Sec. 3 we show our numerical results on the structure of charmed meson–nuclear systems and the formation spectra for them. Section 4 is devoted to the conclusions of this paper.

2. Formalism

First of all, we present the formalism for the formation spectra of charmed meson–nuclear systems in terms of the differential cross sections of the $(\bar{p}, D^+)$ and $(\bar{p}, \bar{D}^0)$ reactions on a nuclear target. In the calculation of the formation spectra, the charmed meson–nucleon scattering amplitudes as well as the charmed meson self-energies and optical potentials are essential. In this study we employ the approach proposed in Refs. [47–49]. The charmed meson–nucleon interaction in matter and the corresponding charmed meson self-energies are presented in Sec. 2.1. Then, in Sec. 2.2 we construct the optical potential for the charmed mesons, that are needed for the solution of the Klein–Gordon equation (KGE) for the charmed meson–nuclear systems, and summarize our procedure to calculate the production cross section in the Green's function method.

2.1. Charmed meson–nucleon scattering amplitudes and charmed meson self-energies

The different charmed meson–nucleon scattering amplitudes in symmetric nuclear matter and the corresponding charmed meson self-energies are obtained following a self-consistent procedure in coupled channels, as described in [47,48] for the D meson and in [49] for $\bar{D}$ meson. Here we summarize the main features.

The s-wave transition charmed meson–nucleon potential of the Bethe–Salpeter equation is derived from an effective Lagrangian that implements HQSS [36–38]. HQSS is an approximate QCD symmetry that treats on equal footing heavy pseudoscalar and vector mesons, such as charmed and bottomed mesons [39–49]. The effective Lagrangian includes the lowest-lying pseudoscalar and vector mesons as well as $1/2^+$ and $3/2^+$ baryons. It reduces to the WT interaction term in the sector where Goldstone bosons are involved and incorporates HQSS in the sector where heavy quarks participate. This SU(6) × HQSS model is justified in view of the reasonable semi-qualitative outcome of the SU(6) extension [50] and on a formal plausibleness on how the SU(4) WT interaction in the heavy pseudoscalar meson–baryon sectors comes out in the vector–meson exchange picture (see for instance Refs. [21,25]).

The extended WT meson–baryon interaction in the coupled meson–baryon basis with total charm C, strangeness S, isospin I and spin J, is given by

$$V_{ij}^{CSIJ}(\sqrt{s}) = D_{ij}^{CSIJ}\,\frac{2\sqrt{s} - M_i - M_j}{4 f_i f_j}\sqrt{\frac{E_i + M_i}{2M_i}}\sqrt{\frac{E_j + M_j}{2M_j}}, \tag{1}$$

where $\sqrt{s}$ is the center of mass (C.M.) energy of the system; E_i and M_i are, respectively, the C.M. on-shell energy and mass of the baryon in the channel i; and f_i is the decay constant of the meson in the i-channel. Symmetry breaking effects are introduced by using physical masses and decay constants. The D_{ij}^{CSIJ} are the matrix elements coming from the group structure of the extended WT interaction.

The amplitudes in nuclear matter, $T^{\rho,CSIJ}(P^0, \boldsymbol{P})$ with $P = (P^0, \boldsymbol{P})$ the total four-momentum, are obtained by solving the on-shell Bethe–Salpeter equation with the tree level amplitude $V^{CSIJ}(\sqrt{s})$:

$$T^{\rho,CSIJ}(P) = \frac{1}{1 - V^{CSIJ}(\sqrt{s})\, G^{\rho,CSIJ}(P)}\, V^{CSIJ}(\sqrt{s}), \tag{2}$$

where the diagonal $G^{\rho,CSIJ}(P)$ matrix accounts for the charmed meson–baryon loop in nuclear matter [47,49]. We focus in the non-strange $S = 0$ and singly charmed $C = 1$ sector, where DN and D^*N are embedded, as well as the $C = -1$ one, with $\bar{D}N$ and $\bar{D}^*N$.[1]

The $D(\bar{D})$ and $D^*(\bar{D}^*)$ self-energies in symmetric nuclear matter, $\Pi(q^0, \boldsymbol{q}; \rho)$, are obtained by summing the different isospin transition amplitudes for $D(\bar{D})N$ and $D^*(\bar{D}^*)N$ over the nucleon Fermi distribution, p_F. For the $D(\bar{D})$ we have

$$\Pi_{D(\bar{D})}(q^0, \boldsymbol{q}; \rho) = \int_{p \le p_F} \frac{d^3p}{(2\pi)^3}\left[T_{D(\bar{D})N}^{\rho,0,1/2}(P^0, \boldsymbol{P}) + 3\, T_{D(\bar{D})N}^{\rho,1,1/2}(P^0, \boldsymbol{P})\right], \tag{3}$$

while for $D^*(\bar{D}^*)$

$$\Pi_{D^*(\bar{D}^*)}(q^0, \boldsymbol{q}; \rho) = \int_{p \le p_F} \frac{d^3p}{(2\pi)^3}\left[\frac{1}{3}\, T_{D^*(\bar{D}^*)N}^{\rho,0,1/2}(P^0, \boldsymbol{P}) + T_{D^*(\bar{D}^*)N}^{\rho,1,1/2}(P^0, \boldsymbol{P}) + \frac{2}{3}\, T_{D^*(\bar{D}^*)N}^{\rho,0,3/2}(P^0, \boldsymbol{P}) + 2\, T_{D^*(\bar{D}^*)N}^{\rho,1,3/2}(P^0, \boldsymbol{P})\right]. \tag{4}$$

In the above equations, $P^0 = q^0 + E_N(\boldsymbol{p})$ and $\boldsymbol{P} = \boldsymbol{q} + \boldsymbol{p}$ are the total energy and momentum of the meson–nucleon pair in the nuclear matter rest frame, and $(q^0, \boldsymbol{q})$ and $(E_N, \boldsymbol{p})$ stand for the energy and momentum of the meson and nucleon, respectively, in that frame. Those self-energies are determined self-consistently since they are obtained from the in-medium amplitudes which contain the meson–baryon loop functions, and those quantities themselves are functions of the self-energies.

[1] Note that D denotes D^+ and D^0, whereas $\bar{D}$ indicates D^- and $\bar{D}^0$.

2.2. Optical potential and formation spectra

In order to calculate the formation spectra of the meson–nucleus bound states, we need the optical potential of a meson in the nucleus. Relying on the local density approximation, we evaluate the optical potential for the D^- (D^0) mesons[2]

$$V_{\rm opt}(r, E_D) = \frac{1}{2m_D}\Pi_{D^-(D^0)}(E_D, \boldsymbol{q}=0; \rho(r)), \tag{5}$$

where r is the distance from the center of the nucleus and E_D is the energy of the charmed meson, i.e. E_D is same as q^0 in Sec. 2.1. The nuclear density $\rho(r)$ is evaluated from the neutron and proton densities. The densities are deconvoluted as in Ref. [3] to account for the proton and neutron finite sizes. The details on the proton and neutron densities are given in Appendix A.

With the optical potential $V_{\rm opt}$ we can obtain the meson wave function in the nucleus by solving the KGE

$$[-\nabla^2 + \mu^2 + 2\mu V_{\rm opt}(r, E_D - V_{\rm coul}(r))]\phi(\boldsymbol{r}) = [E_D - V_{\rm coul}(r)]^2\phi(\boldsymbol{r}), \tag{6}$$

with μ the D meson–nucleus reduced mass. Here $V_{\rm coul}(r)$ is the Coulomb potential given by

$$V_{\rm coul}(r) = e^2 Z_D \int \frac{\rho_{\rm ch}(r')}{|\boldsymbol{r}-\boldsymbol{r}'|}d^3r', \tag{7}$$

where e is the elementary charge, Z_D is the charge of the charmed meson, and $\rho_{\rm ch}(r)$ is the charge distribution of the nucleus of Eq. (A.1). We note that, for the D^0-nucleus system, the Coulomb interaction is automatically removed, since $Z_D = 0$.

Next we discuss the procedure to calculate the formation spectra in terms of the differential cross sections in the Green's function method [51]. The details of the Green's function method can be found in Refs. [52–56], and here we only summarize the main features.

In this work, we calculate the formation spectra of the D^-–, D^0–^{11}B systems in the

$$\bar{p} + {}^{12}{\rm C} \to \left[{}^{11}{\rm B} - D^-\right] + D^+, \tag{8}$$

$$\bar{p} + {}^{12}{\rm C} \to \left[{}^{11}{\rm B} - D^0\right] + \bar{D}^0 \tag{9}$$

reactions. As mentioned in the introduction, these processes are of interest for the forthcoming experiments by the PANDA and CBM Collaborations at the future FAIR facility and in J-PARC. For simplicity, we concentrate on the formation spectra of the $(\bar{p}, \bar{D})$ process.

The present method starts with the separation of the cross section into the nuclear response function $S(E_D)$ and the elementary cross section for the $p(\bar{p}, \bar{D})D$ reaction within the impulse approximation for D meson production

$$\left(\frac{d^2\sigma}{d\Omega dE_D}\right)_{A(\bar{p},\bar{D})(A-1)\otimes D} = \left(\frac{d\sigma}{d\Omega}\right)^{\rm LAB}_{p(\bar{p},\bar{D})D} \times S(E_D). \tag{10}$$

The differential cross section of the elementary process $p(\bar{p}, \bar{D})D$ in the laboratory frame (LAB), $(d\sigma/d\Omega)^{\rm LAB}_{p(\bar{p},\bar{D})D}$, can be evaluated using some appropriate models or be taken from experimental data. For this cross section, we will use the theoretical results of Ref. [57]. The nuclear response function $S(E_D)$ contains information on the dynamics between D-meson and the final $(A-1)$ nucleus. To calculate the nuclear response function, we employ the Green's function method. Namely, the nuclear response function with a complex potential is formulated in Ref. [51] as

$$S(E_D) = -\frac{1}{\pi}{\rm Im}\sum_f \int d^3r d^3r' \tau_f^\dagger(\boldsymbol{r}) G(E_D; \boldsymbol{r}, \boldsymbol{r}')\tau_f(\boldsymbol{r}'), \tag{11}$$

where τ_f denotes the transition amplitude of the initial state $\bar{p} + {}^A Z$ to the proton–hole final nucleus and the outgoing $D - \bar{D}$ meson pair, and $G(E_D; \boldsymbol{r}, \boldsymbol{r}')$ is the Green's function of the D meson interacting with the nucleus. The summation is taken over all possible final states f. The Green's function $G(E_D; \boldsymbol{r}, \boldsymbol{r}')$ is defined as,

$$G(E_D; \boldsymbol{r}, \boldsymbol{r}') = \langle\alpha|\phi(\boldsymbol{r})\frac{1}{E_D - H_D + i\epsilon}\phi^\dagger(\boldsymbol{r}')|\alpha\rangle, \tag{12}$$

where α indicates the proton–hole state, H_D is the Hamiltonian of the D meson–nucleus system, and $\phi^\dagger(\boldsymbol{r})$ is the D meson creation operator. The transition amplitude τ_f involves the proton–hole wave function ψ_{j_N} and the distorted waves χ_i and χ_f of the projectile and ejectile, respectively. The distorted waves are calculated within the eikonal approximation as

$$\chi_f^*(\boldsymbol{r})\chi_i(\boldsymbol{r}) = \exp(i\boldsymbol{q}\cdot\boldsymbol{r})F(\boldsymbol{r}), \tag{13}$$

with the momentum transfer $\boldsymbol{q}$ and the distortion factor $F(\boldsymbol{r})$ defined as

$$F(\boldsymbol{r}) = \exp\left[-\frac{1}{2}\bar{\sigma}\int_{-\infty}^{\infty} dz'\bar{\rho}(z', \boldsymbol{r})\right], \tag{14}$$

where $\bar{\sigma}$ is the averaged cross section

$$\bar{\sigma} = \frac{\sigma_{\bar{p}N} + \sigma_{\bar{D}N}}{2}, \tag{15}$$

with $\sigma_{\bar{p}N}$ and $\sigma_{\bar{D}N}$, the total $\bar{p}N$ and DN cross sections, respectively. We use the values $\sigma_{\bar{p}N} = 59$ mb, and $\sigma_{\bar{D}N} = 10$ mb obtained in the theoretical calculation of Ref. [30]. Besides, the averaged nuclear density, $\bar{\rho}$, is approximated by that of the ^{11}B nucleus (Eq. (A.5)). By performing the spin sums, the amplitude τ_f can be written as,

$$\tau_f(\boldsymbol{r}) = \chi_f^*(\boldsymbol{r})\xi^*_{1/2,m_s}[Y^*_{l_\phi}(\hat{r}) \otimes \psi_{j_N}(\boldsymbol{r})]_{JM}\,\chi_i(\boldsymbol{r}), \tag{16}$$

where it appears also the D-meson angular wave function $Y_{l_\phi}(\hat{r})$, which depends on the direction of the vector $\boldsymbol{r}$ ($\hat{r}$), and the spin wave function $\xi_{1/2,m_s}$ of the outgoing $\bar{D}$-meson. We assume harmonic oscillator wave functions for the proton–hole ψ_{j_N} wave function calculated with an empirical value of range parameter. We stress that within this approach, the D-nucleus optical potential only enters in the Hamiltonian H_D that appears in the Green's function.

3. Numerical results

Next, we show our numerical results for the structure and formation spectra of the D^-- and D^0-nucleus bound states. In the present calculation, we focus on the $^{12}{\rm C}(\bar{p}, D^+)$ and $^{12}{\rm C}(\bar{p}, \bar{D}^0)$ reactions, and thus we consider the $[D^- - {}^{11}{\rm B}]$ and $[D^0 - {}^{11}{\rm B}]$ systems. After discussing the properties of the charmed meson–nucleus bound states obtained by solving the KGE in Sec. 3.1, we show the formation spectra for these states in Sec. 3.2.

[2] For the calculation of the D^- optical potential we do not vary the subtraction point, namely $\alpha = 1$, and we do not consider the nucleon extraction energy (or gap) (see [49] for details).

Table 1
Binding energies B_E and widths Γ of D^- atomic states in ^{11}B.

State	Coulomb only	Coulomb + optical	
	B_E [keV]	B_E [keV]	Γ [keV]
1s	844.8	446.1	77.0
2s	236.1	162.5	17.0
3s	108.9	83.7	6.3
4s	62.4	50.9	3.0
2p	264.4	249.7	9.7
3p	117.4	112.3	3.3
4p	66.0	63.8	1.5
3d	117.6	117.6	6.0
4d	66.1	66.1	3.5
4f	66.0	66.0	2.5

Table 2
Binding energies B_E and widths Γ of D^- and D^0 nuclear states in ^{11}B.

State	D^- meson		D^0 meson	
	B_E [MeV]	Γ [MeV]	B_E [MeV]	Γ [MeV]
1s	21.7	0.5	6.5	10.8
2p	14.5	2.4	–	–

3.1. Atomic and nuclear charmed meson bound states in ^{11}B

Binding energy ($B_E > 0$) and width (Γ) of the charmed meson–^{11}B bound states are related to the eigenenergy appearing in Eq. (6) by $E_D = \mu - B_E - i\Gamma/2$. Since the D^- or $\bar{D}^0$ meson optical potential $V_{opt}(r, E_D)$ depends on the energy, we have self-consistently solved the KGE [48,49]. We start by discussing the D^- atomic levels in ^{11}B, which are Coulomb assisted bound states. The found levels are compiled in Table 1, where we show both the results obtained only with the Coulomb potential and those obtained when the optical potential is added to the Coulomb interaction. We can see that the inclusion of the strong interaction leads to smaller binding energies for both s and p orbital states compared to the corresponding values obtained when only the Coulomb interaction is considered. This is to say, the strong interaction between the D^--meson and the ^{11}B nucleus is repulsive in this case. This is caused by the level repulsion induced by the existence of nuclear bound s and p states. In addition, the imaginary part of the optical potential has a well-known repulsive effect, also seen in [49]. We emphasize that the decay widths are smaller than the binding energies thanks to the absence of strong decay channels for the D^-N pair,[3] which implies that such D^- atomic states may be observed in dedicated experiments.

Next, we search for charmed meson–nuclear bound states originated from the strong interaction via the optical potential. Binding energies and decay widths are listed in Table 2. We find 1s and 2p nuclear states for $[D^-$–^{11}B] and a 1s nuclear state for the $[D^0$–^{11}B] system. The binding energies turn out to be around ten MeV or more. We find narrow widths for the D^- mesic nuclear states,[4] however the decay width of the D^0 mesic nuclear state is larger than its binding energy. This is due to the existence of open strong decay modes ($\Sigma_c\pi$, $\Lambda_c\pi$) of the DN pair. The natural question that arises is whether these mesic nuclear states will appear in the spectrum of the one proton pick-up reactions. We address this issue in the next subsection.

[3] Indeed, the small widths in the medium are due to the excitation of particle–hole, i.e., $\bar{D} \to \bar{D}NN^{-1}$ [49].

[4] Note that it is expected that $\bar{D}^0$ nuclear states will resemble those of D^- due to isospin symmetry, as seen in Ref. [49].

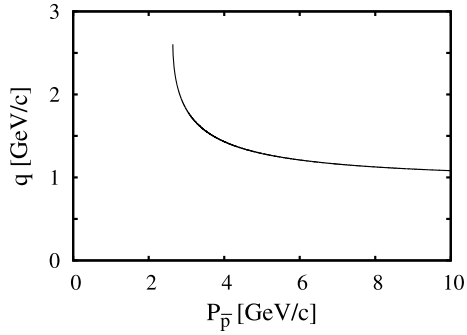

Fig. 1. Momentum transfer (LAB frame) as a function of the antiproton momentum in the $^{12}C(\bar{p}, \bar{D})$ reaction.

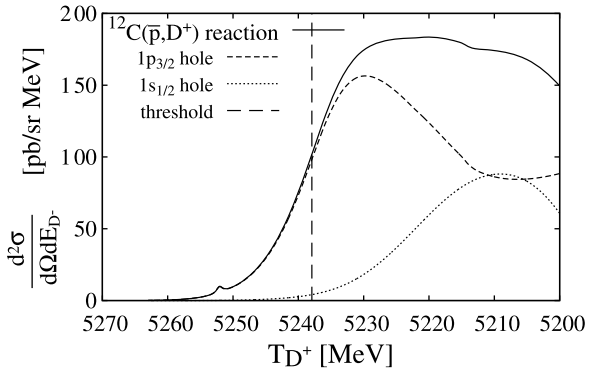

Fig. 2. Formation spectrum for the $\bar{p} + {}^{12}C \to [{}^{11}B - D^-] + D^+$ reaction at $P_{\bar{p}} =$ 8 GeV/c and $\theta^{LAB}_{D^+} = 0°$, as a function of the outgoing D^+ meson total energy. The partial contributions of some shell configurations of the final nucleus are also shown in the figure. The vertical dashed line indicates the D^- meson production threshold.

3.2. Formation spectra

We calculate the formation spectra of the $[D^-$–^{11}B] and $[D^0$–^{11}B] systems. We produce these states in the $^{12}C(\bar{p}, D^+)$ and $^{12}C(\bar{p}, \bar{D}^0)$ reactions, respectively (Eqs. (8) and (9)). We consider forward scattering for the outgoing D^+ or $\bar{D}^0$ meson to maximally suppress the momentum transferred to the mesic nuclear or atomic bound states. Using this kinematics, we show in Fig. 1 the momentum transfer in these reactions as a function of the antiproton momentum, $P_{\bar{p}}$, in the LAB frame. We see that a large momentum transfer about 1 GeV/c is inevitable when working with an antiproton beam.

In this preliminary study we fix the LAB antiproton momentum to 8 GeV/c, since we expect to obtain in this region, both a large elementary cross section [58] and a momentum transfer close to the smallest possible, as seen in Fig. 1. On the other hand, we use the theoretical results of Ref. [57] for the differential cross section of the elementary process $(d\sigma/d\Omega)^{LAB}$ at forward angle of the outgoing $D^+/\bar{D}^0$ meson. Thus, at $P_{\bar{p}} = 8$ GeV/c, we take 760 nb/sr (40 nb/sr) for the $p\bar{p} \to D^+D^-$ ($p\bar{p} \to D^0\bar{D}^0$) reaction.

In Fig. 2, we show the formation spectrum of the $[D^-$–^{11}B] system as a function of the outgoing D^+ meson total energy (T_{D^+}) in the LAB frame. We can appreciate a bump structure around $T_{D^+} = 5250$ MeV placed below the D^- production threshold. It comes from the contribution of the $1p_{3/2}$ hole configuration of ^{11}B, and the peak corresponds to the 2p state of the $[D^-$–^{11}B] nuclear state found in the previous subsection. However, its strength is very small compared to the quasifree contribution above the D^- production threshold ($T_{D^+} > 5238$ MeV), mainly due to the very large momentum transfer in the reaction. The cross section for

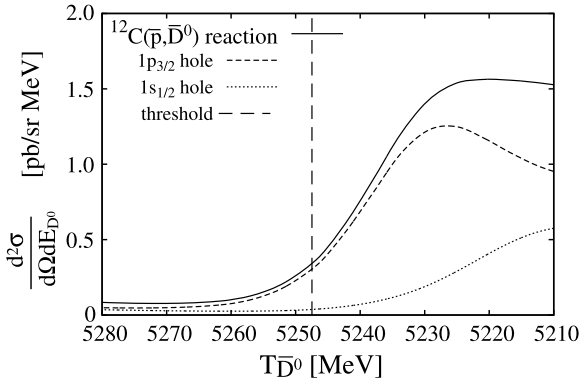

Fig. 3. Same as in Fig. 2, but for the $\bar{p}+{}^{12}\mathrm{C}\to\left[{}^{11}\mathrm{B}-D^0\right]+\bar{D}^0$ reaction. The vertical dashed line indicates now the D^0 meson production threshold.

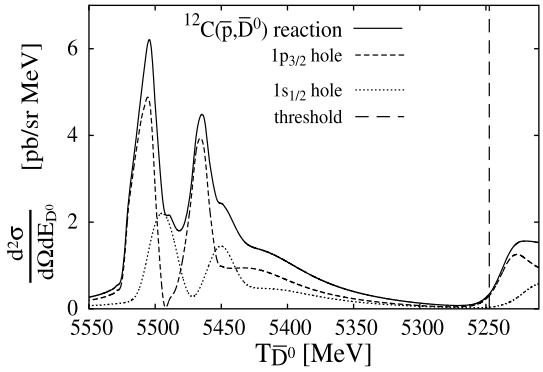

Fig. 4. As in Fig. 3, but covering the region of very deep D^0 binding energies.

the reaction is proportional to $|\Phi_{nlm}(q)|^2$, where $\Phi_{nlm}(q)$ is the D^- bound wave function in momentum space [59–62]. The cross sections are small because the D^- bound wave function has difficulty to accommodate such large momentum of around 1 GeV. Given the expected typical size of the D^- bound states (similar to D^0 in Ref. [48]), momentum components significantly larger than 0.4–0.5 GeV in the D^- bound wave function are already expected to be small. Thus, one gets a large suppression form factor. The large momentum transfer also leads to the disappearance of the $1s$ state below the $2p$ state in the formation spectrum, since the $1s_{1/2}$ hole contribution is negligible in the bound region.[5]

In Fig. 3 we show now the formation spectrum of the $[D^0$–$^{11}\mathrm{B}]$ system as a function of the outgoing $\bar{D}^0$ meson total energy ($T_{\bar{D}^0}$) in the LAB frame. In this case, we do not see in the formation spectrum any signature of the $1s$ nuclear state with $B_E = 6.5$ MeV reported in Table 2. This is again because of the large momentum transfer of the reaction. However, we note that we find two peaks in formation spectrum for $\bar{D}^0$ energies in the region of 5.5 GeV, which would correspond to very deeply bound D^0 states. These structures are shown in Fig. 4, but we do not obtain any eigenstates in such deep energy region. These peaks in the formation spectrum come from the energy dependence of the optical potential, as can be seen in Fig. 5, and they are associated to the dynamically-generated $\Sigma_c(2556)$-hole and $\Lambda_c(2595)$-hole states, as discussed in [47].

As already noted, the rather large momentum transfer involved in the $\bar{p}+p\to D+\bar{D}$ reactions tends to hinder the formation

[5] Due to the large momentum transfer, the convergence of the formation spectrum above the threshold becomes very slow and we have needed to sum up to fifteen D^--nucleus partial waves.

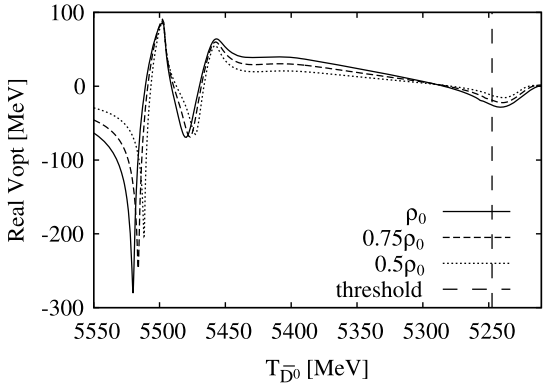

Fig. 5. D^0–^{11}B optical potential [47] for several nuclear densities in terms of the nuclear matter saturation density, ρ_0, as a function of the D^0 meson energy.

process. Much smaller momentum transfers can be achieved with alternative reactions. For instance,

$$\bar{p}+p\to D^{*-}+D^+,$$
$$D^{*-}+A_Z\to\pi^0+\left[A_Z-D^-\right]_{\mathrm{b}}. \tag{17}$$

After emission of a pion the charmed meson can be slow and get trapped by the nucleus. More generally, in reactions of the type $\bar{p}+N\to\bar{D}^*+D$ followed by $\bar{D}^*\to\bar{D}+\pi$ or $\bar{p}+N\to\bar{D}+D^*$ followed by $D^*\to D+\pi$, the vector meson may be real or virtual and the D or $\bar{D}$ produced may be slow and get trapped. (Note that nothing prevents the antiproton to annihilate with the neutrons instead of the protons of the nucleus, thereby increasing the reaction cross section.) Likewise, bremsstrahlung of pions produced by the antiproton as it impacts the nucleus also changes the kinematics and could lead to new formation mechanisms. All these alternative mechanisms in which energy and momentum is released by emission of pions (or even photons) could help to reduce the momentum transfer to the final charmed meson and are therefore worth studying. From the theoretical point of view we would expect sizeable formation peaks over a flat background.

4. Conclusions

In this work we have calculated the formation spectra of the charmed/anti-charmed mesic nuclear states in the $^{12}\mathrm{C}(\bar{p},D^+)$ and $^{12}\mathrm{C}(\bar{p},\bar{D}^0)$ antiproton reactions, aiming to provide useful information for experiments such as PANDA in the future FAIR facility and J-PARC. There exists also the possibility of observing these exotic mesic nuclei in relativistic heavy-ion collisions, such as those taking place in the future CBM experiment at FAIR.

For this purpose, we have described the (anti-)charmed meson–nucleon scattering amplitude in dense matter by employing a unitarized coupled-channels model based on an extended WT interaction to account for HQSS constraints in the charm sector. Then, with the (anti-)charmed meson–nucleon amplitude in matter, we have constructed the self-energies and, hence, optical potentials of the (anti-)charmed mesons in ^{11}B. Solving the KGE with the D^- and D^0 optical potentials in ^{11}B, we have found $1s$ and $2p$ nuclear states for the D^- case and only the $1s$ level for the D^0 case, in addition to the atomic states for D^-. Of special interest is the fact that the anti-charmed $[D^-$–$^{11}\mathrm{B}]$ nuclear states have very small decay widths from quasi-elastic $D^-N\to\bar{D}N'$ collisions.

Next, we have calculated the charmed and anti-charmed mesic nuclear formation spectra in the $^{12}\mathrm{C}(\bar{p},D^+)$ and $^{12}\mathrm{C}(\bar{p},\bar{D}^0)$ reactions by employing the Green's function method. The momentum of the antiproton beam has been fixed to 8 GeV/c, and the final mesons $D^+/\bar{D}^0$ are taken in the forward direction to suppress as

much as possible the momentum transferred to the mesic nuclear bound states. We have found, on the one hand, that the $2p$ D^- nuclear state may show up in the formation spectrum as a small peak. However, its peak strength is very small compared to the quasifree contribution above the D^- production threshold, mainly due to the very large momentum transfer in the reaction. The large momentum transfer also leads to the disappearance of the $1s$ state below the $2p$ state in the formation spectrum for D^-. On the other hand, for the D^0 meson, the nuclear bound state does not lead to any visible signatures in the spectrum, although at deep energy regions large peaks are present. These structures correspond to the dynamically-generated $\Sigma_c(2556)$-hole and $\Lambda_c(2595)$-hole excitations, and their experimental observation might shed light into the dynamics of these resonances inside of a nuclear environment.

Finally we note that in the $(\bar{p}, D^+)$ and $(\bar{p}, \bar{D}^0)$ reactions, the momentum transfer is inevitably large. Therefore, in order to have visible strengths for the $1s$ or $2p$ nuclear states, we should consider different production reactions with small momentum transfer. One possibility is to examine the $(\bar{p}, D+N)$ and $(\bar{p}, D+2N)$ reactions, with a much smaller or even zero momentum transfer, although the formation cross sections could be suppressed as well because of the complexity of the reaction mechanisms. Other competing formation mechanisms could involve the emission of pions by real or virtual intermediate D^* or $\bar{D}^*$ with subsequent trapping of the slow pseudoscalar charmed meson by the final nucleus.

Acknowledgements

We acknowledge the support by Open Partnership Joint Projects of JSPS Bilateral Joint Research Projects. This research has been supported by the Spanish Ministerio de Economía y Competitividad and European FEDER funds under the contracts FIS2011-28853-C02-02, FPA2013-43425-P, FIS2014-51948-C2-1-P, FIS2014-59386-P, FIS2014-57026-REDT and SEV-2014-0398. Also, this work has been financed by Generalitat Valenciana under contract PROMETEOII/2014/0068, by Junta de Andalucía (grant FQM225), and by the EU HadronPhysics3 project, grant agreement No. 283286. LT acknowledges support from the Ramón y Cajal Research Programme from Ministerio de Economía y Competitividad.

Appendix A. Neutron and proton densities

For the evaluation of the nuclear density $\rho(r)$ of a given nucleus, one has to obtain the neutron and proton densities. Namely for the ^{11}B nucleus, on the one hand, the charge distribution $\rho_{\rm ch}$ is given by a modified harmonic oscillator (MHO) distribution

$$\rho_{\rm ch}(r) = \rho_0 \left[1 + a\left(\frac{r}{R}\right)^2\right] \exp\left[-\left(\frac{r}{R}\right)^2\right]. \tag{A.1}$$

The neutron matter distribution is taken to be identical to $\rho_{\rm ch}$. On the other hand, the densities of proton (ρ_p) and neutron (ρ_n) turn out to have also a MHO shape [3], but with modified parameters to account for the proton and neutron finite sizes,

$$\rho_{p,n}(r) = \rho_0' \left[1 + a'\left(\frac{r}{R'}\right)^2\right] \exp\left[-\left(\frac{r}{R'}\right)^2\right], \tag{A.2}$$

with the parameters a' and R' given by

$$a' = \frac{2x}{2-3x}, \quad x = \frac{aR^2}{1+3a/2}\frac{1}{R'^2}, \tag{A.3}$$

$$R' = \sqrt{R^2 - \frac{2}{3}\langle r_{p,n}\rangle^2}, \tag{A.4}$$

with the mean radius of the proton or neutron $\langle r_{p,n}^2\rangle = 0.69$ fm^2. Then the nuclear density ρ is the sum of the proton and neutron densities:

$$\rho(r) = \rho_p(r) + \rho_n(r). \tag{A.5}$$

We use $R = 1.69$ fm and $a = 0.811$, and the normalization factors ρ_0 and ρ_0' are determined so that $\int d^3r \rho_{\rm ch}(r) = \int d^3r \rho_p(r) = 5$, and $\int d^3r \rho_n(r) = 6$.

References

[1] M. Ericson, T.E.O. Ericson, Ann. Phys. 36 (1966) 323.
[2] E. Friedman, A. Gal, Phys. Rep. 452 (2007) 89.
[3] J. Nieves, E. Oset, C. Garcia-Recio, Nucl. Phys. A 554 (1993) 509.
[4] C. Garcia-Recio, J. Nieves, E. Oset, Nucl. Phys. A 547 (1992) 473.
[5] S. Hirenzaki, Mod. Phys. Lett. A 23 (2008) 2497.
[6] H. Gilg, A. Gillitzer, M. Knulle, M. Munch, W. Schott, P. Kienle, K. Itahashi, K. Oyama, et al., Phys. Rev. C 62 (2000) 025201.
[7] S. Wycech, F.J. Hartmann, J. Jastrzebski, B. Klos, A. Trzcinska, T. von Egidy, Phys. Rev. C 76 (2007) 034316.
[8] B. Klos, A. Trzcinska, J. Jastrzebski, T. Czosnyka, M. Kisielinski, P. Lubinski, P. Napiorkowski, L. Pienkowski, et al., Phys. Rev. C 76 (2007) 014311.
[9] A. Trzcinska, J. Jastrzebski, P. Lubinski, F.J. Hartmann, R. Schmidt, T. von Egidy, B. Klos, Phys. Rev. Lett. 87 (2001) 082501.
[10] http://www.fair-center.eu/public/experiment-program.html.
[11] http://j-parc.jp/researcher/Hadron/en/index.html.
[12] K. Tsushima, D.H. Lu, A.W. Thomas, K. Saito, R.H. Landau, Phys. Rev. C 59 (1999) 2824.
[13] P.A.M. Guichon, Phys. Lett. B 200 (1988) 235.
[14] S. Yasui, K. Sudoh, Phys. Rev. C 87 (2013) 015202.
[15] S. Yasui, K. Sudoh, Phys. Rev. D 80 (2009) 034008.
[16] Y. Yamaguchi, S. Yasui, A. Hosaka, Nucl. Phys. A 927 (2014) 110.
[17] M. Bayar, C.W. Xiao, T. Hyodo, A. Dote, M. Oka, E. Oset, Phys. Rev. C 86 (2012) 044004.
[18] L. Tolos, J. Schaffner-Bielich, A. Mishra, Phys. Rev. C 70 (2004) 025203.
[19] L. Tolos, J. Schaffner-Bielich, H. Stoecker, Phys. Lett. B 635 (2006) 85.
[20] M.F.M. Lutz, E.E. Kolomeitsev, Nucl. Phys. A 730 (2004) 110.
[21] M.F.M. Lutz, E.E. Kolomeitsev, Nucl. Phys. A 755 (2005) 29.
[22] J. Hofmann, M.F.M. Lutz, Nucl. Phys. A 763 (2005) 90.
[23] J. Hofmann, M.F.M. Lutz, Nucl. Phys. A 776 (2006) 17.
[24] M.F.M. Lutz, C.L. Korpa, Phys. Lett. B 633 (2006) 43.
[25] T. Mizutani, A. Ramos, Phys. Rev. C 74 (2006) 065201.
[26] L. Tolos, A. Ramos, T. Mizutani, Phys. Rev. C 77 (2008) 015207.
[27] C.E. Jimenez-Tejero, A. Ramos, I. Vidana, Phys. Rev. C 80 (2009) 055206.
[28] C.E. Jimenez-Tejero, A. Ramos, L. Tolos, I. Vidana, Phys. Rev. C 84 (2011) 015208.
[29] J. Haidenbauer, G. Krein, U.G. Meissner, A. Sibirtsev, Eur. Phys. J. A 33 (2007) 107.
[30] J. Haidenbauer, G. Krein, U.G. Meissner, A. Sibirtsev, Eur. Phys. J. A 37 (2008) 55.
[31] J. Haidenbauer, G. Krein, U.G. Meissner, L. Tolos, Eur. Phys. J. A 47 (2011) 18.
[32] J.-J. Wu, R. Molina, E. Oset, B.S. Zou, Phys. Rev. Lett. 105 (2010) 232001.
[33] J.-J. Wu, R. Molina, E. Oset, B.S. Zou, Phys. Rev. C 84 (2011) 015202.
[34] J.-J. Wu, T.-S.H. Lee, B.S. Zou, Phys. Rev. C 85 (2012) 044002.
[35] E. Oset, A. Ramos, E.J. Garzon, R. Molina, L. Tolos, C.W. Xiao, J.J. Wu, B.S. Zou, Int. J. Mod. Phys. E 21 (2012) 1230011.
[36] N. Isgur, M.B. Wise, Phys. Lett. B 232 (1989) 113.
[37] M. Neubert, Phys. Rep. 245 (1994) 259.
[38] A.V. Manohar, M.B. Wise, Heavy Quark Physics, Camb. Monogr. Part. Phys. Nucl. Phys. Cosmol., vol. 10, 2007.
[39] C. Garcia-Recio, V.K. Magas, T. Mizutani, J. Nieves, A. Ramos, L.L. Salcedo, L. Tolos, Phys. Rev. D 79 (2009) 054004.
[40] D. Gamermann, C. Garcia-Recio, J. Nieves, L.L. Salcedo, L. Tolos, Phys. Rev. D 81 (2010) 094016.
[41] O. Romanets, L. Tolos, C. Garcia-Recio, J. Nieves, L.L. Salcedo, R.G.E. Timmermans, Phys. Rev. D 85 (2012) 114032.
[42] C. Garcia-Recio, J. Nieves, O. Romanets, L.L. Salcedo, L. Tolos, Phys. Rev. D 87 (2013) 034032.
[43] C. Garcia-Recio, J. Nieves, O. Romanets, L.L. Salcedo, L. Tolos, Phys. Rev. D 87 (2013) 074034.
[44] L. Tolos, Int. J. Mod. Phys. E 22 (2013) 1330027.
[45] C.W. Xiao, J. Nieves, E. Oset, Phys. Rev. D 88 (2013) 056012.
[46] A. Ozpineci, C.W. Xiao, E. Oset, Phys. Rev. D 88 (2013) 034018.
[47] L. Tolos, C. Garcia-Recio, J. Nieves, Phys. Rev. C 80 (2009) 065202.
[48] C. Garcia-Recio, J. Nieves, L. Tolos, Phys. Lett. B 690 (2010) 369.
[49] C. Garcia-Recio, J. Nieves, L.L. Salcedo, L. Tolos, Phys. Rev. C 85 (2012) 025203.
[50] D. Gamermann, C. Garcia-Recio, J. Nieves, L.L. Salcedo, Phys. Rev. D 84 (2011) 056017.

[51] O. Morimatsu, K. Yazaki, Nucl. Phys. A 435 (1985) 727.
[52] R.S. Hayano, S. Hirenzaki, A. Gillitzer, Eur. Phys. J. A 6 (1999) 99.
[53] F. Klingl, T. Waas, W. Weise, Nucl. Phys. A 650 (1999) 299.
[54] D. Jido, H. Nagahiro, S. Hirenzaki, Phys. Rev. C 66 (2002) 045202.
[55] H. Nagahiro, D. Jido, S. Hirenzaki, Phys. Rev. C 68 (2003) 035205.
[56] H. Nagahiro, D. Jido, S. Hirenzaki, Nucl. Phys. A 761 (2005) 92.
[57] J. Haidenbauer, G. Krein, Phys. Rev. D 89 (2014) 114003.
[58] A.B. Kaidalov, P.E. Volkovitsky, Z. Phys. C 63 (1994) 517.
[59] J. Nieves, E. Oset, Nucl. Phys. A 518 (1990) 617.
[60] S. Hirenzaki, H. Toki, T. Yamazaki, Phys. Rev. C 44 (1991) 2472.
[61] J. Nieves, E. Oset, Phys. Lett. B 282 (1992) 24.
[62] K. Itahashi, et al., Phys. Rev. C 62 (2000) 025202.